




Distinguishability and mixedness in quantum interference

Alex E. Jones ^{1,*} Shreya Kumar,^{2,3,*} Simone D'Aurelio ^{2,3} Matthias Bayerbach ^{2,3}
Adrian J. Menssen,⁴ and Stefanie Barz^{2,3,†}

¹*Quantum Engineering Technology Labs, H. H. Wills Physics Laboratory and Department of Electrical and Electronic Engineering, University of Bristol, Bristol BS8 1FD, United Kingdom*

²*Institute for Functional Matter and Quantum Technologies, University of Stuttgart, 70569 Stuttgart, Germany*

³*Center for Integrated Quantum Science and Technology (IQST), University of Stuttgart, 70569 Stuttgart, Germany*

⁴*Research Laboratory of Electronics, Massachusetts Institute of Technology, Cambridge, Massachusetts 02139, USA*



(Received 15 January 2023; accepted 2 October 2023; published 1 November 2023)

We study the impact of distinguishability and mixedness, two fundamental properties of quantum states, on quantum interference. We show that these can influence the interference of multiple particles in different ways, leading to effects that cannot be observed in the interference of two particles alone. This is demonstrated experimentally by interfering three independent photons in pure and mixed states and observing their different multiphoton interference, despite exhibiting the same two-photon Hong-Ou-Mandel interference. In addition to its fundamental relevance, our observation has important implications for quantum technologies relying on photon interference.

DOI: [10.1103/PhysRevA.108.053701](https://doi.org/10.1103/PhysRevA.108.053701)

I. INTRODUCTION

Quantum interference is a defining feature of quantum physics, leading to behavior that puts it in sharp contrast to its classical counterpart. Beyond its importance on a fundamental level, interference is also a crucial component for many modern quantum technologies. For example, those relying on photon interference include photonic quantum computing, boson sampling approaches to demonstrating quantum advantage, quantum metrology and quantum networks [1–7]. However, quantum interference suffers from an intrinsic trade-off between which-path information and interference strength [8,9]. Therefore, a key requirement for high-quality operation of these technologies is that the photons are indistinguishable and have a high purity. Otherwise, the quantum interference degrades and this leads to a reduction in the fidelity of quantum operations.

Extensive theoretical and experimental work has been developed for analyzing the effect of photon distinguishability in computationally demanding tasks like boson sampling [10–24]. A common approach to quantifying similarity of photons is to perform a Hong-Ou-Mandel (HOM) interference test between pairs of them. One photon is injected into each input of a balanced beam splitter and the relative time delay is varied over the coherence time of the photons' wavepackets [25]. The visibility of the variation in coincidence counts gives

a measure of the overlap of the photons' wave functions, and so can characterize the similarity and quality of photons [26]. The existence of distinguishable states can give rise to another important photon error: mixedness, where a photon is in an incoherent combination of different states. This also leads to decreased interference strength. Existing theoretical work captures the effects of both of these errors but qualitative differences between the resulting behavior are unclear [10,12,27].

Here, we show that discrimination between distinguishability and purity in the interference of independent photons requires at least three photons. We demonstrate this experimentally by preparing sets of three photons in pure and mixed states and interfering them in a multiport splitter. We use intuitive geometric interpretations to show that, in both cases, the HOM visibilities are the same, but other multiphoton output statistics differ. Our result underscores that two-particle interferences are generally insufficient for predicting the nature of interference in larger systems of mixed quantum states.

II. DISTINGUISHABLE AND MIXED STATES

A photon's state is defined by its mode. We will make a distinction between the *resolved* degrees of freedom where detectors do resolve the mode structure (in our case, the spatial mode) and the *unresolved* degrees of freedom where they do not (here, the temporal mode and polarization). We will investigate distinguishability in interference by starting with a set of independent photons, prepared with one photon per spatial mode, and states that determine their distinguishability. The photons then evolve through an interferometer that mixes spatial modes but leaves other degrees of freedom unchanged. Finally, the photons are detected at the outputs.

*These authors contributed equally to this work.

†Corresponding author: stefanie.barz@fmq.uni-stuttgart.de

Published by the American Physical Society under the terms of the [Creative Commons Attribution 4.0 International license](https://creativecommons.org/licenses/by/4.0/). Further distribution of this work must maintain attribution to the author(s) and the published article's title, journal citation, and DOI.

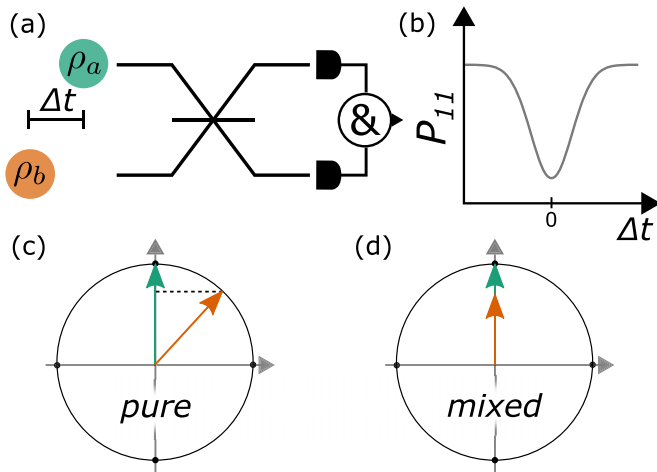


FIG. 1. (a) HOM dip measurement where photons with states ρ_a and ρ_b and relative time delay Δt interfere on a balanced beam splitter. (b) We here assume the photons occupy identical Gaussian wavepackets. The output coincidence probability P_{11} reaches a minimum at zero relative delay and the visibility depends on the overlap of their states. For a two-dimensional space where ρ_a is assumed pure, this overlap of Bloch vectors is reduced by (c) distinguishability and (d) mixedness in the same way, giving identical HOM dip visibilities.

If photons differ in their unresolved states then there is, in principle, information that can distinguish between the photon paths in an interferometer leading to a particular output pattern [10–12]. For example, in HOM interference the relative arrival time of two photons at a beam splitter allows discrimination between the two paths leading to output coincidence detection, namely, both photons being transmitted or both being reflected. As the relative time delay approaches zero, the paths become indistinguishable. This strengthens the destructive interference that suppresses output coincidences and leads to a characteristic HOM dip [see Figs. 1(a) and 1(b)].

If the two photons instead have pure states $|a\rangle$ and $|b\rangle$ that are different in some other unresolved degree of freedom besides arrival time, then the strength of coincidence suppression at zero relative delay is determined by the pairwise distinguishability $|\langle a|b\rangle|^2$. This can be measured using the HOM dip visibility $\mathcal{V} = (\max - \min)/\max$. The introduction of a third photon with state $|c\rangle$ means there are four distinguishing parameters: three pairwise distinguishabilities and the appearance of a multiparticle phase $\varphi_{abc} = \arg(\langle a|b\rangle\langle b|c\rangle\langle c|a\rangle)$ [15]. Adding more photons leads to more pairwise distinguishabilities and additional multiparticle phases with a similar form. For N pure photons, at most $(N - 1)^2$ real parameters describe their distinguishability [13, 16].

More generally, quantum systems such as photons can be in mixed states. For example, heralding from a spectrally entangled pair source leads to mixed photon states. The similarity of two photons in states ρ_a and ρ_b is then described by the real pairwise trace $\text{Tr}(\rho_a\rho_b)$. Extending to more photons, similarity is related to traces of products of their density matrices and mixedness means the largest number of distinguishing parameters for N coincident photons increases to $(N! - 1)$ [12, 28]. Constructing pure state decompositions

for the mixed states involved means that interference can be expressed as an incoherent sum of pure state interferences [10]. However, this obscures intuitive aspects of interference that can be captured through geometric considerations of the distinguishing parameters. In this paper, we investigate the form of these parameters for two and three photons and show how distinguishability and mixedness can affect multiphoton interference differently.

III. TWO-PHOTON INTERFERENCE

We begin by showing that two-photon interference visibility does not discriminate between distinguishability and mixedness. Consider two photons with states ρ_a and ρ_b impinging on a balanced beam splitter. If the probability of observing output coincidences P_{11} is monitored as the relative time delay is varied, a HOM dip is observed [Figs. 1(a) and 1(b)]. Its visibility is determined by the pairwise trace $\text{Tr}(\rho_a\rho_b)$. This quantity can be interpreted geometrically by considering an unresolved space with two dimensions; here the minimum number needed for two photons to exhibit complete distinguishability.

Let Bloch vectors \mathbf{r}_a and \mathbf{r}_b describe the states ρ_a and ρ_b , respectively, so $\mathbf{r}_j = \text{Tr}(\rho_j\boldsymbol{\sigma})$, $j = a, b$, where $\boldsymbol{\sigma}$ is the vector of Pauli matrices. The pairwise trace is related to the dot product as

$$\text{Tr}(\rho_a\rho_b) = \frac{1}{2}(1 + \mathbf{r}_a \cdot \mathbf{r}_b). \quad (1)$$

The lengths and relative orientation of the Bloch vectors describe the purities and distinguishability of the states, respectively, and affect the pairwise trace in the same way [see Figs. 1(c) and 1(d)]. This also holds for two vectors describing unresolved states in a higher-dimensional space, where the dot product determines the pairwise trace. Thus, the visibility of HOM interference between two independent photons cannot discriminate between distinguishability and mixedness.

IV. THREE-PHOTON INTERFERENCE

The interference of three photons depends on five distinguishing parameters: three real pairwise traces and also the generally *complex* triple trace $\text{Tr}(\rho_a\rho_b\rho_c)$. Here we consider qubit states that permit an intuitive geometric description of the triple trace. Associating a Bloch vector \mathbf{r}_j to each state ρ_j , $j = a, b, c$, we find [29]

$$\text{Tr}(\rho_a\rho_b\rho_c) = \frac{1}{4}(1 + \mathbf{r}_a \cdot \mathbf{r}_b + \mathbf{r}_a \cdot \mathbf{r}_c + \mathbf{r}_b \cdot \mathbf{r}_c + iV_{abc}). \quad (2)$$

The dot products describe pairwise similarities and the imaginary component encodes a collective description via the scalar triple product of the three Bloch vectors: $V_{abc} = \mathbf{r}_a \cdot (\mathbf{r}_b \times \mathbf{r}_c)$. This has a magnitude given by the volume of the corresponding parallelepiped and a sign set by its orientation in a right-handed frame [see Fig. 2(a)]. It is also antisymmetric under pairwise swaps of the vectors. If the Bloch vectors are coplanar then $V_{abc} = 0$ and the triple trace is real and fully determined by pairwise traces. Otherwise, it contains information not captured by the dot products alone.

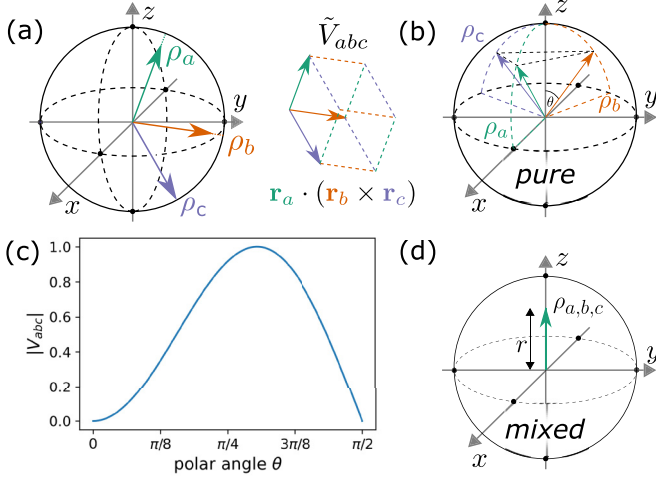


FIG. 2. (a) The scalar triple product of three Bloch vectors V_{abc} encodes a collective description of the states. (b) Pure qubit states equally spaced in azimuthal angle but with varying θ [Eq. (3)]. (c) Magnitude of the volume V_{abc} for the pure state preparation. (d) Mixed states where pairwise similarity is controlled by purity through the vector length r [Eq. (4)].

V. PURE AND MIXED PREPARATIONS OF THREE PHOTONS

We now consider two preparations of three photons: one where pairwise similarities are governed by distinguishability and another where they are determined by state purity. HOM visibilities for the two preparations could be the same, but we will see that V_{abc} plays an important role in three-photon interference.

We define orthogonal states $\{|0\rangle, |1\rangle\}$ to span the unresolved qubit space. These could correspond to a basis for polarization or spectral differences, for example. Here we encode these qubits using horizontal and vertical polarisations $\{|H\rangle, |V\rangle\}$. First, we consider three photons in pure states

$$\begin{aligned} |a\rangle &= \cos(\theta/2)|H\rangle + \sin(\theta/2)|V\rangle, \\ |b\rangle &= \cos(\theta/2)|H\rangle + e^{i\frac{2\pi}{3}}\sin(\theta/2)|V\rangle, \\ |c\rangle &= \cos(\theta/2)|H\rangle + e^{i\frac{4\pi}{3}}\sin(\theta/2)|V\rangle, \end{aligned} \quad (3)$$

with $0 \leq \theta \leq \pi/2$. These vectors lie at the top of the Bloch sphere when $\theta = 0$ and are equally spaced in the equator when $\theta = \pi/2$. Like the petals of a blooming flower, for other values of θ they point between the top of the Bloch sphere and the equator, and remain equally spaced in azimuthal angle, as shown in Fig. 2(b). For these pure states, $\rho_j = |j\rangle\langle j|$, $j = a, b, c$, and the three pairwise traces are equal and given by $\text{Tr}(\rho_j\rho_k) = (5 + 3\cos 2\theta)/8$; they vary between 0.25 and 1. The volume $V_{abc} = -3\sqrt{3}/2 \times \cos\theta \sin^2\theta$ and its magnitude varies between 0 and 1, as shown in Fig. 2(c).

The second preparation we consider uses identical mixed states to vary the pairwise similarity solely by purity. Each photon has the same state

$$\rho_p = p|H\rangle\langle H| + (1-p)|V\rangle\langle V|. \quad (4)$$

p is the preparation probability, the length of the Bloch vector is $r = |2p - 1|$, and the state purity is $\mathcal{P} = \frac{1}{2}(1 + r^2)$ [see Fig. 2(d)]. Here the pairwise traces are again equal and now given by the purity, varying between 0.5 and 1, and overlapping with the range possible for the pure state configuration. However, crucially V_{abc} is here always zero.

VI. MULTIPHOTON INTERFERENCE STATISTICS

To investigate how the various distinguishing parameters manifest in interference, we consider interfering these preparations of three photons in a balanced three-port interferometer. This “tritter” is described by a unitary matrix with elements $U_{j,k} = \exp(jk\frac{2\pi i}{3})/\sqrt{3}$. When photons with qubit states labeled a, b, c enter inputs 1–3 respectively, the probabilities of various output patterns are (Appendix A)

$$\begin{aligned} P_{111} &= \frac{1}{18}(3 + \mathbf{r}_a \cdot \mathbf{r}_b + \mathbf{r}_a \cdot \mathbf{r}_c + \mathbf{r}_b \cdot \mathbf{r}_c), \\ P_{(120)} &= \frac{1}{36}(3 - \mathbf{r}_a \cdot \mathbf{r}_b - \mathbf{r}_a \cdot \mathbf{r}_c - \mathbf{r}_b \cdot \mathbf{r}_c - \sqrt{3}V_{abc}), \\ P_{(210)} &= \frac{1}{36}(3 - \mathbf{r}_a \cdot \mathbf{r}_b - \mathbf{r}_a \cdot \mathbf{r}_c - \mathbf{r}_b \cdot \mathbf{r}_c + \sqrt{3}V_{abc}), \\ P_{(300)} &= \frac{2}{3}P_{111}. \end{aligned} \quad (5)$$

The subscripts indicate the numbers of photons in the individual output modes. The brackets around the output configurations denote those related by cyclic permutation of occupation numbers, so $(210) = \{210, 102, 021\}$. The dot products of Bloch vectors derive from the interference of paths related by the pairwise exchange of photons and dependence on V_{abc} comes from interfering paths related by full permutation of photons. The high symmetry of the tritter is the reason why all fully bunched probabilities are the same, and why the partially bunched probabilities look similar. The probabilities of coincidences P_{111} and of bunchings $P_{(300)}$ depend linearly on the dot products of Bloch vectors and are not sensitive V_{abc} . This observation and its extension to larger systems are discussed in Appendix B. Critically, here, the partially bunched probabilities depend on V_{abc} .

VII. EXPERIMENT AND RESULTS

We generate photons using a pair of periodically poled potassium titanyl phosphate (ppKTP) crystals designed for degenerate spontaneous parametric down-conversion (SPDC) at 1550 nm. We prepare the photons’ polarizations using sets of wave plates, interfere them in a fiber tritter, and detect them using superconducting nanowire single-photon detectors (SNSPDs). Further details of the experimental setup are given in Fig. 3 and Appendix C.

We first prepare three photons in the pure states of Eq. (3) [shown in Fig. 2(b)]. The angle θ is varied from 0 to $\pi/2$ using wave plates. This monotonically decreases the pairwise trace $\text{Tr}(\rho_j\rho_k)$ from 1 to 0.25. θ also changes the volume $|V_{abc}|$ as shown in Fig. 2(c). We then perform two sets of measurements: first, two-photon interference dips are recorded between pairs of photons interfering in the tritter. These tritter HOM (THOM) dips have half the visibility of the corresponding standard HOM dips, so can also be used to infer pairwise traces. Second, three-photon counts at the tritter outputs are used to estimate the three-photon scattering

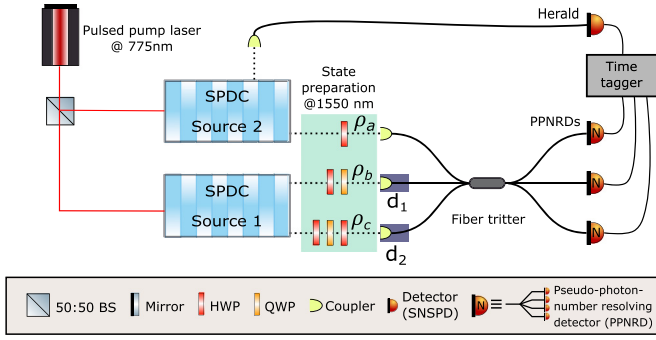


FIG. 3. A laser pumps two SPDC sources to generate indistinguishable photons. Both photons emitted from Source 1 enter the tritter and Source 2 is operated in a heralded configuration to supply a third photon. The photons' polarizations are prepared using sets of half-wave plates (HWPs) and quarter-wave plates (QWPs) and arrival times are matched using delay stages d_1 and d_2 . Details of polarization control are given in Appendix C. Each tritter output is connected to a four-port splitter for pseudo-photon-number resolution. At the measurement stage, all outputs are connected to superconducting nanowire single-photon detectors (SNSPDs) with $>90\%$ efficiencies and then a time tagger is used to count the different photon statistics.

probabilities. In Fig. 4(a) we plot a selection of partially bunched scattering probabilities against the associated HOM visibility between photon pairs, along with theory curves. From Eq. (5), these three-photon probabilities depend on pairwise traces and also on V_{abc} . The first leads to a linear contribution to the probabilities as the pairwise trace varies and the second to nonmonotonic variation. Next, we use the six partially bunched probabilities and the expressions in Eq. (5) to estimate the magnitude $|V_{abc}|$ for each value of θ . This is plotted against the HOM visibility in Fig. 4(b) and displays the nonmonotonic variation expected for the manipulation of V_{abc} in Fig. 2(c).

Next, we simulate the preparation of three photons in the mixed states of Eq. (4) [shown in Fig. 2(d)]. We achieve this by measuring three-photon counts for all eight input combinations where each photon has H or V polarization. Summing these with appropriate weightings depending on preparation probability p simulates the scattering for photons in identical mixed states. We select a set of pairwise traces between 0.5 and 1 for which we determine three-photon scattering probabilities. We plot some of the partially bunched probabilities against HOM visibilities in Fig. 4(c) with ideal theory curves. Their behavior contrasts sharply with that for the pure state preparation by following a linear relation with pairwise traces because the volume $V_{abc} = 0$. We use partially bunched

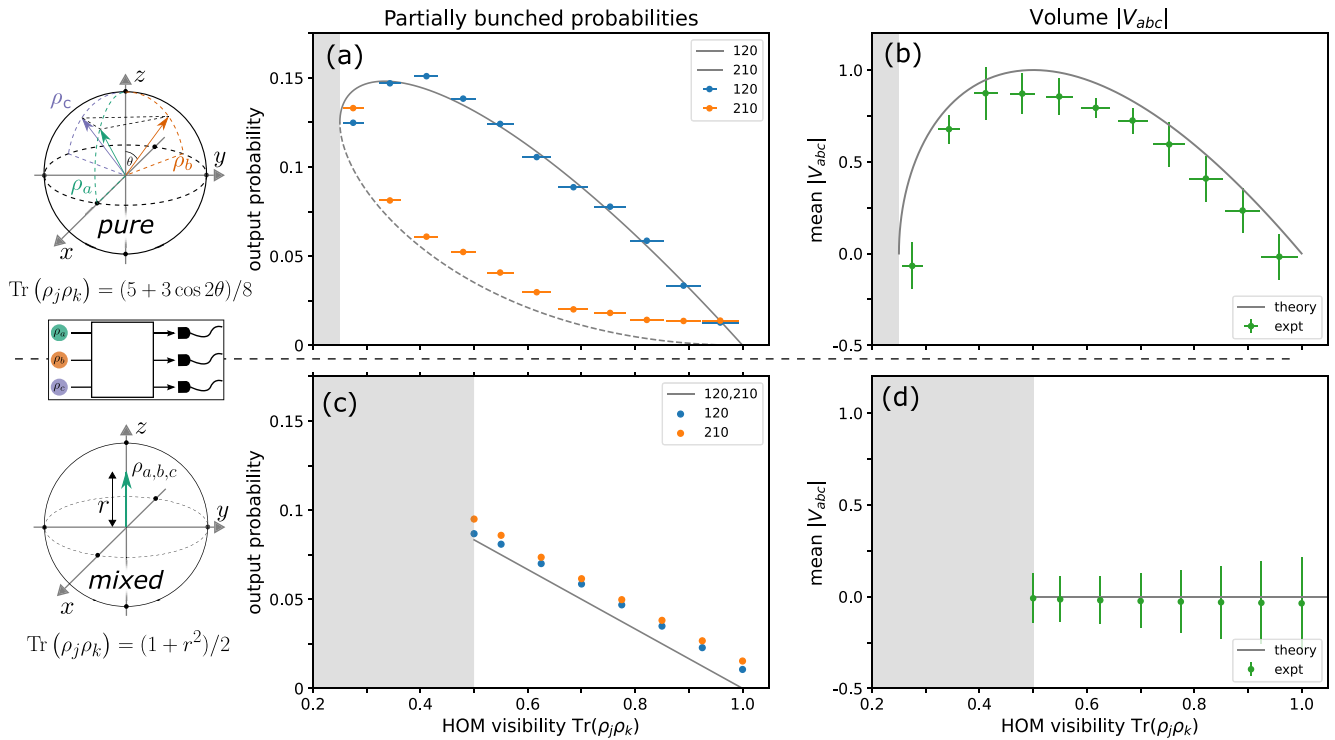


FIG. 4. Partially bunched probabilities and extracted volumes $|V_{abc}|$ for pure [top row (a), (b)] and mixed [bottom row (c), (d)] preparations of three photons interfering in a tritter. Gray regions indicate values of the pairwise trace that cannot be accessed for each preparation, and gray curves are ideal theory. For the top row, the pairwise traces of the interfering photons vary between 1 and 0.25 as the angle θ varies from 0 to $\pi/2$. From Eq. (5), partially bunched probabilities depend on V_{abc} and so vary nonmonotonically. In (b) we estimate $|V_{abc}|$ using the six partially bunched probabilities and plot it against the associated HOM visibility. For the bottom row, the pairwise traces are determined by the state purity that varies between 0.5 and 1 as the Bloch vector length r varies from 0 to 1. Here $V_{abc} = 0$ and so the partially bunched statistics in (c) vary linearly with the pairwise trace. Horizontal error bars in the top plots are determined experimentally from mean THOM visibilities. Vertical error bars in (a,c) are comparable to marker size, and in (b,d) arise from differences in estimates from the partially bunched probabilities. Additional three-photon data for other output patterns are given in Appendix D.

probabilities to estimate V_{abc} as the state purity is varied, and find it is zero throughout, as shown in Fig. 4(d).

Differences between the experimental results and ideal theory in Fig. 4 are due to imperfect state preparation, residual spectral distinguishability and mixedness, and higher-order photon emissions from the SPDC sources. Also, we use four-port splitters for pseudo-photon-number resolution and imbalances in their splitting ratio will affect the probabilities determined from photon counts.

The key takeaway from Fig. 4 is that the two very different preparations of photons can give rise to the same (T)HOM dip visibilities but different three-photon probabilities. Both preparations access pairwise traces of between 0.5 and 1 (as indicated by overlapping regions of the shared x axis) and so (T)HOM experiments cannot discriminate between them (two-photon data are given in Appendix E). Also, the coincident and fully bunched probabilities only depend on pairwise traces and so also cannot distinguish the state preparations, as shown by additional data in Appendix D. However, partially bunched probabilities depend on V_{abc} and so, as shown by Figs. 4(b) and 4(d), can distinguish between preparations of photons in a way impossible using lower-order interference.

This interference test is not intended as a general diagnostic tool for identifying mixedness. However, in Appendix F we show that measurement of HOM visibilities and V_{abc} can permit identification of mixedness for specific state preparations. In addition to discriminating between these special state preparations, we find measurement of HOM visibilities and V_{abc} can also be used to identify mixedness of the interfering qubit states.

VIII. DISCUSSION

In this work, we presented an experiment that reveals the different effects of distinguishability and mixedness in multiphoton interference beyond two photons. The scalar triple product of Bloch vectors embodies this for unresolved qubit states.

We can briefly comment on how the investigations here extend to more photons and higher dimensions. Adding a fourth photon with a qubit state ρ_d introduces a dependence on $\text{Tr}(\rho_a\rho_b\rho_c\rho_d)$. However, as shown in Appendix G, this depends only on dot products and scalar triple products of Bloch vectors, and so this four-photon interference is fully described by two- and three-photon parameters. This holds for the interference of any number of independent photons with qubit states. The choice of qubit states here imposes a restriction on the five parameters governing three-photon interference (see Appendix F). Turning to higher dimensions, qutrits are sufficient to fully probe all parameters. The triple trace then contains extra terms [30–32] so that, unlike for qubits, HOM visibilities do not fully determine the real part of the triple trace, as shown in Appendix H.

Our result highlights the importance of going beyond HOM visibilities when characterising photon indistinguishability. Here, the sensitivity to V_{abc} was crucial to discriminating photon preparations. This is particularly relevant in the context of photonic quantum technologies, where much effort is dedicated to engineering sources of pure, indistinguishable photons. Common approaches include spontaneous processes

that rely on material nonlinearities, such as spontaneous parametric down-conversion and four-wave mixing, and here residual correlations can lead to mixed single photons. We note that the two-dimensional space used here was to allow intuition at small scales, but generally mixedness will be over larger spaces. Other, in principle, deterministic quantum emitters, such as quantum dots, can be difficult to align, resulting in spectral distinguishability. The choice of photon source will determine the dominant photon errors, necessitating careful characterization to determine the impact on quantum operation fidelity, for example, photonic Bell-state generation [33].

Beyond tests of quantum computational complexity using photons [3,34], optical approaches to universal measurement-based quantum computation rely on the generation of small entangled states that can be combined to build up a cluster resource state [35,36]. The effect of photon distinguishability on fault-tolerant schemes has been investigated [37], but a more general treatment also including effects of photon impurity (and routes to protect against such errors) will become crucial as the scale of optical quantum technologies continues to grow. As well as photons, our work also applies to systems of other interfering particles where interactions with the environment and which-path information can degrade indistinguishability.

ACKNOWLEDGMENTS

We thank M. Tichy and H. Chrzanowski for useful discussions. We acknowledge support from the Carl Zeiss Foundation, the Centre for Integrated Quantum Science and Technology (IQST), the German Research Foundation (DFG), the Federal Ministry of Education and Research (BMBF, project SiSiQ), and the Federal Ministry for Economic Affairs and Energy (BMWi, project PlanQK). A.E.J is supported by the EPSRC Hub in Quantum Computing and Simulation (EP/T001062/1). A.J.M. acknowledges support from the Feodor Lynen fellowship of the Humboldt Foundation, MITRE Quantum Moonshot and the DARPA ONISQ programs.

APPENDIX A: CALCULATING SCATTERING PROBABILITIES

If single photons with states ρ_i , $i = 1, \dots, N$ are input into the i th arms of an N -mode interferometer, the probability of a detection outcome is given by [10,12]

$$P_{\rho_1, \dots, \rho_N} = \mathcal{N} \sum_{\sigma \in S_N} \left[\left(\prod_{j=1}^a \text{Tr}(\rho_{\alpha_{j1}} \dots \rho_{\alpha_{jn}}) \right) \times \text{perm}(M \star M_{\sigma, \mathbb{1}}^*) \right], \quad (\text{A1})$$

where $(\alpha_{j1}, \dots, \alpha_{jn})$ is the structure of the j th disjoint cycle of σ , where σ is an element of the permutation group S_N . a is the number of disjoint cycles in σ , n is the length of the j th cycle, and M is the scattering matrix constructed from the input and output mode occupations. Here \star indicates the element-wise product of matrix elements. For an

input state configuration with photon number occupations n_i , $r = (n_1, n_2, \dots, n_i, \dots, n_m)$, the mode assignment list $d(r)$ is defined as

$$d(r) = \underbrace{(1, \dots, 1)}_{n_1\text{-times}}, \underbrace{(2, \dots, 2)}_{n_2\text{-times}}, \dots, \underbrace{(m, \dots, m)}_{n_m\text{-times}}, \quad (\text{A2})$$

which contain the mode indices for each photon as many times as the number of photons occupying that mode. We similarly define the mode assigned list $d(s)$ for the output state configuration $s = (l_1, l_2, \dots, l_i, \dots, l_m)$. The scattering matrix M is then constructed from the unitary U as $M = U_{d(r), d(s)}$. The normalization \mathcal{N} is given by: $\mathcal{N} = (\prod_j s_j! r_j!)^{-1}$.

APPENDIX B: INSENSITIVITY OF COINCIDENT AND FULLY BUNCHED STATISTICS TO V_{abc}

The coincident and fully bunched probabilities shown in Fig. 4 for a tritter interferometer depend linearly on the pairwise traces and exhibit no dependence on the volume V_{abc} [defined for the pure state preparation in Figs. 2(b) and 2(c)]. This actually holds for any three-port unitary interferometer.

For scattering probabilities to exhibit sensitivity to the imaginary components of traces of density matrices, the expression in Eq. (A1) should change under $\rho_j \rightarrow \rho_j^*$. n -photon interference depends on $\text{Tr}(\rho_{\alpha_{j_1}} \dots \rho_{\alpha_{j_n}})$, where $(\alpha_{j_1}, \dots, \alpha_{j_n})$ is the j th disjoint cycle of some permutation σ . Under complex conjugation of all ρ_j we find

$$[\text{Tr}(\rho_{\alpha_{j_1}} \dots \rho_{\alpha_{j_n}})]^* = \text{Tr}(\rho_{\alpha_{j_n}} \dots \rho_{\alpha_{j_1}}). \quad (\text{B1})$$

The density matrices in the trace are now permuted according to the j th disjoint cycle of the inverse permutation σ^{-1} . n -photon interference in Eq. (A1) therefore depends on

$$\begin{aligned} & \text{Tr}(\rho_{\alpha_{j_1}} \dots \rho_{\alpha_{j_n}}) \times \text{perm}(M \star M_{\sigma, \mathbb{I}}^*) \\ & + \text{Tr}(\rho_{\alpha_{j_1}} \dots \rho_{\alpha_{j_n}})^* \times \text{perm}(M \star M_{\sigma^{-1}, \mathbb{I}}^*). \end{aligned} \quad (\text{B2})$$

For the case of three-photon coincidences from a three-port unitary interferometer U , the scattering matrix $M = U$. Inserting the Euler angle decomposition for a general SU(3) unitary [38] reveals that these permanents are purely real. Hence coincidences here are not sensitive to the imaginary part of $\text{Tr}(\rho_a \rho_b \rho_c)$ and so exhibit no dependence on V_{abc} . For more than three photons this condition does not necessarily hold: N -photon coincidence probabilities, where $N > 3$, can be sensitive to imaginary components of traces of density matrices.

For fully bunched probabilities where all N photons occupy the k th output port, the scattering matrix M is constructed by taking the k th column of the unitary describing the interferometer N times. The element-wise product $M \star M_{\sigma, \mathbb{I}}^*$ yields a real matrix and so a real permanent. Therefore, fully bunched probabilities do not depend on imaginary parts of the traces of density matrices, and so in the three-photon case do not depend on V_{abc} .

APPENDIX C: EXPERIMENTAL SETUP

The setup is shown in Fig. 5. A mode-locked Ti:sapphire laser with a repetition rate of 76 MHz emits 3.2-ps pulses centered at 775 nm. It is used to pump two periodically

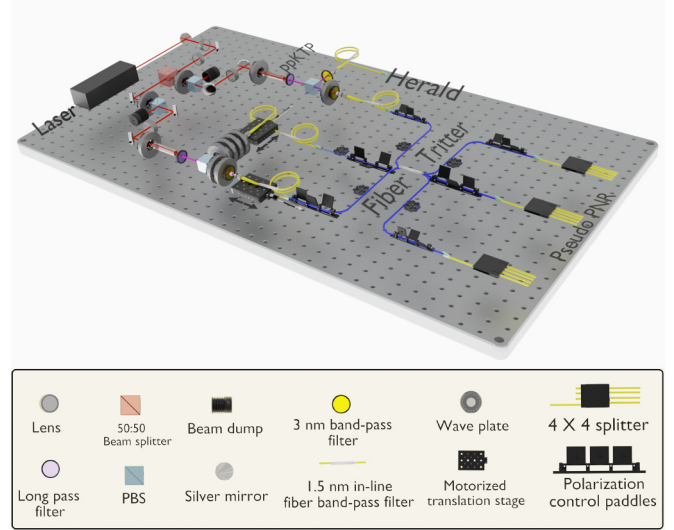


FIG. 5. Detailed experimental setup described in the main text of Appendix C.

poled potassium titanyl phosphate (ppKTP) crystals of dimensions $1 \text{ mm} \times 1 \text{ mm} \times 30 \text{ mm}$ and a poling period of $\Lambda = 46.175 \mu\text{m}$. The pump power is controlled by a combination of a HWP and a polarizing beam splitter (PBS) before being divided into two beams using a 50 : 50 beam splitter. After additional power control, the beams are focused onto the crystals using a combination of lenses, resulting in an ideal beam waist at the crystals. HWPs before the crystals ensure the polarization required for the phase-matching condition. The crystals are placed in temperature-controlled ovens to set the temperature for ideal degenerate phase-matching.

After the crystals, longpass filters are used to block the pump beam; 3-nm and 1.5-nm bandpass filters centered at 1550 nm are used to ensure spectral indistinguishability, which is verified by measuring the photons' spectra using a spectrometer (Kymera 193i-B1 spectrometer and iDus In-GaAs DU490A-1.7 photo-diode array by Andor Technology). The signal and idler photons are orthogonally polarised and are separated using PBSs. A linear polarizer is used to clean the polarization in the reflected arm of the PBS. HWPs and QWPs are then used to set the photons' polarisations. Delay stages temporally align the photons, which are then coupled into single-mode fibers. Polarization states undergo random rotations on propagating through optical fiber. We compensate for these using paddles such that the desired polarization states interfere at the tritter, up to some global unitary that does not affect relative orientations of the states. In our setup, both sources were pumped with an average power of 50 mW, which is low enough to reduce the effect of higher-order emissions while maintaining good count rates. We obtain an average rate for four-photon events of $\approx 10 \text{ Hz}$. This allows for shorter integration times per measurement, thereby reducing the effect of environmental changes.

A classical laser light at 1550 nm was used to characterize the tritter. Table I shows the splitting ratio at different output ports with respect to the total output power. The insertion loss is determined for each input port by taking the ratio of power sent in to the tritter to the net power at the output of the tritter.

TABLE I. Splitting ratio and insertion loss of the tritter.

	Output 1	Output 2	Output 3	Insertion loss
Input 1	32.01%	30.24%	29.86%	0.356 dB
Input 2	33.05%	29.18%	29.75%	0.363 dB
Input 3	32.97%	27.92%	29.94%	0.409 dB

These losses are mostly due to the connectors used (E2000 connectors) that are rated to have a loss of the order of 0.5 dB.

We apply the Sinkhorn-Knopp algorithm [39] to the data in Table I to recover the normalized magnitudes for the scattering matrix elements, effectively correcting for imbalanced losses. We then use a minimization procedure to find the phases that ensure unitarity of the tritter scattering matrix, and find

$$U_{\text{tritter}}^{\text{Exp}} = \frac{1}{\sqrt{3}} \begin{pmatrix} 0.987 & 1.02 & 0.997 \\ 1.00 & 0.999e^{2.11i} & 0.997e^{-2.07i} \\ 1.01 & 0.984e^{-2.09i} & 1.01e^{2.09i} \end{pmatrix}. \quad (\text{C1})$$

This has very high fidelity with the ideal tritter and so we use the ideal scattering matrix in our analysis. We verified the polarization independence of the interferometer by recovering the same splitting probabilities for horizontally and vertically polarized light.

APPENDIX D: ADDITIONAL THREE-PHOTON DATA

In Figs. 4(a) and 4(c) of the main text we plotted two of the partially bunched tritter output probabilities for each state preparation. In Fig. 6, we plot all the partially bunched, coincident, and fully bunched probabilities.

APPENDIX E: TRITTER HOMS DIPS AND PAIRWISE TRACES FOR THREE-PHOTON EXPERIMENTS

The two preparations of three photons presented in Eqs. (3) and (4) of the main text are chosen so that they cannot be discriminated by THOM visibilities alone. Alongside the three-photon data shown in Fig. 4, we also record sets of THOM dips and use their visibilities to infer the pairwise traces of pairs of interfering photons. Note that the two-photon coincidence probability through an ideal tritter is $P_{11} = [2 - \text{Tr}(\rho_j \rho_k)]/9$, and so here the maximum visibility of an indistinguishable THOM dip is $\mathcal{V} = 0.5$. The associated HOM visibility on a balanced beam splitter is simply twice the THOM visibility.

As an example, we choose a pairwise trace of $\text{Tr}(\rho_j \rho_k) = 0.7$. This corresponds to $\theta = 0.684$ in the pure preparation of Eq. (3) and a preparation probability $p = 0.816$ in the mixed preparation of Eq. (4). In the later case we simulate impurity by incoherently summing counts for the four combinations of input pairs of photons each in H or V polarization. The results are shown in Fig. 7. The key observation is that the THOM

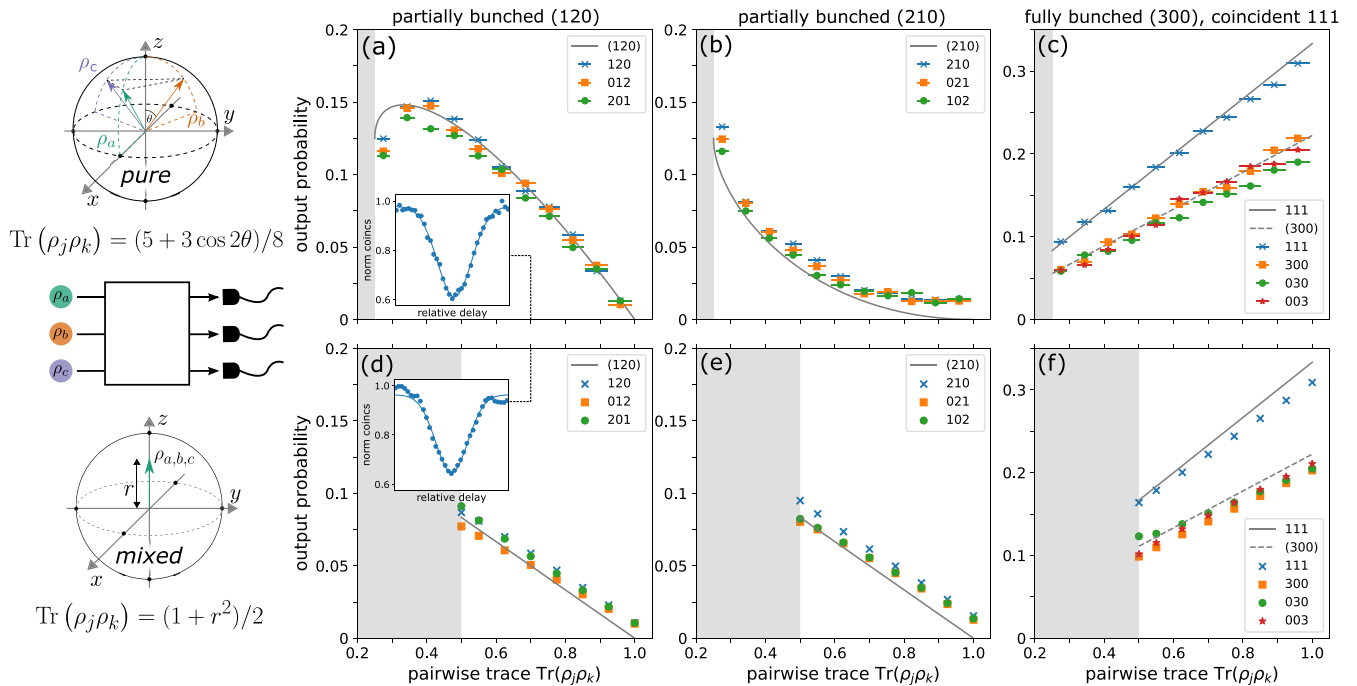


FIG. 6. Scattering probabilities for pure [top row (a)–(c)] and mixed [bottom row (d)–(f)] preparations of three photons interfering in a tritter. Gray regions indicate values of the pairwise trace that cannot be accessed for each preparation and gray curves are ideal theory. For the top row, the pairwise traces of the interfering photons vary between 1 and 0.25 as the angle θ varies from 0 to $\pi/2$. From Eq. (5), partially bunched probabilities (a) and (b) depend differently on V_{abc} , but in (c) the fully bunched and coincidence probabilities depend only on pairwise traces. For the bottom row, the pairwise traces are determined by the state purity that varies between 0.5 and 1 as the Bloch vector length r varies from 0 to 1. Here $V_{abc} = 0$ and so the partially bunched statistics in (d) and (e) vary linearly with the pairwise trace, like the other probabilities in (f). Inset THOM dips for a given pairwise trace cannot discriminate between the state preparations. Horizontal error bars in the top plots are determined experimentally from mean THOM visibilities and all vertical error bars are comparable to marker size.

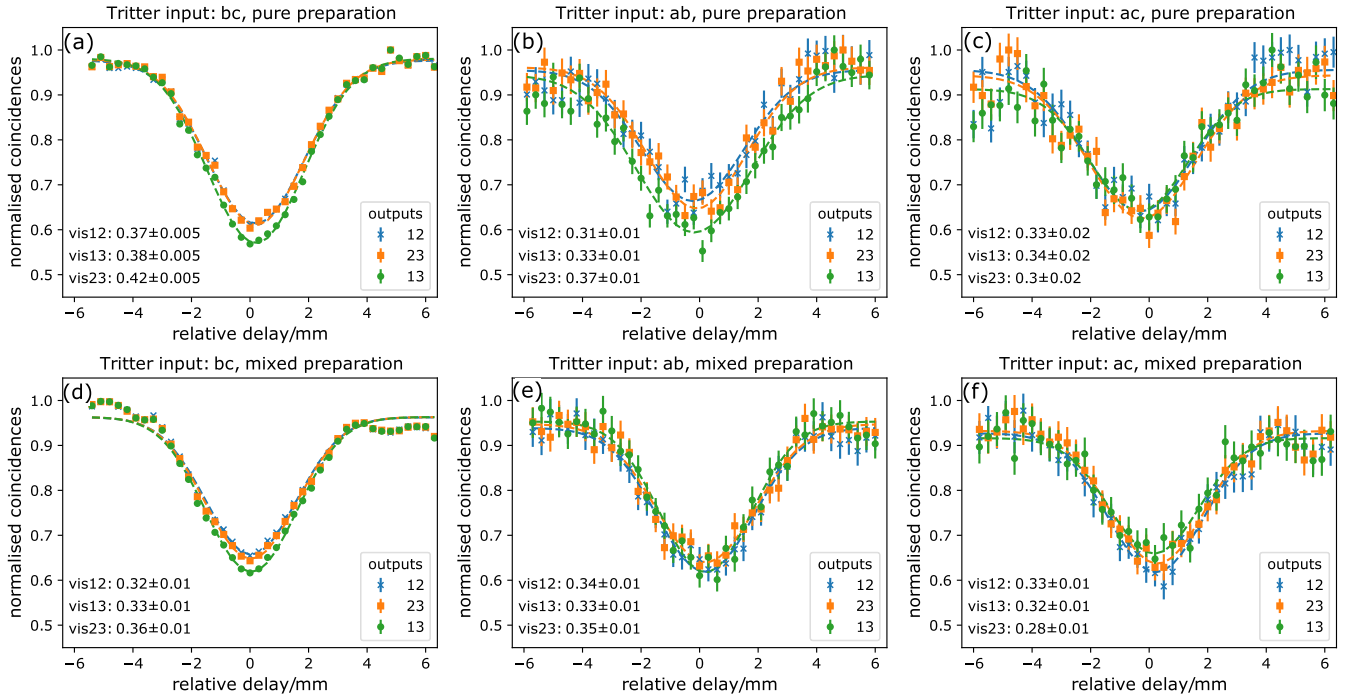


FIG. 7. Experimental THOM dips for pairs of photons from the pure [top row (a)–(c)] and mixed [bottom row (d)–(f)] preparations of photons, with pairwise traces set to $\text{Tr}(\rho_j \rho_k) = 0.7$. Error bars are from Poissonian statistics [smaller for the single source twofolds in (a), (d)], dashed lines are fits to the data, and quoted visibilities and errors are determined from these fits.

visibilities are the same for the pure preparation in the top row and the mixed preparation in the bottom row.

To confirm the accuracy of our pure state preparation, we fit all sets of THOM dips and plot the inferred pairwise traces against the ideal values. To a good approximation we assume an ideal tritter, so the pairwise trace is given by twice the associated THOM visibility. Results are shown in Fig. 8. Differences between ideal and experimental values are due to slight variations in the paths around the Bloch sphere depicted

in Fig. 2(b), likely arising from small errors in wave-plate calibration. We measured THOM dip visibilities for six of the eleven θ values used in Figs. 4(a) to 4(c). A linear fit is used to estimate pairwise traces that were not measured experimentally. The means of these pairwise traces and their errors are used for the x coordinates and errors in Figs. 4 and 6.

APPENDIX F: USING V_{abc} TO IDENTIFY MIXEDNESS FOR QUBITS

We can determine V_{abc} using multiphoton statistics and here we show how it permits identification of mixedness. Its magnitude is given by [40]

$$|V_{abc}| = r_a r_b r_c [1 - (\hat{r}_a \cdot \hat{r}_b)^2 - (\hat{r}_a \cdot \hat{r}_c)^2 - (\hat{r}_b \cdot \hat{r}_c)^2 + 2(\hat{r}_a \cdot \hat{r}_b)(\hat{r}_a \cdot \hat{r}_c)(\hat{r}_b \cdot \hat{r}_c)]^{\frac{1}{2}}, \quad (\text{F1})$$

where r_i is the length of vector \mathbf{r}_i and $\hat{\mathbf{r}}_i = \mathbf{r}_i/r_i$ are unit vectors. For pure qubits, $r_i = 1$ and the magnitude $|V_{abc}|$ is completely determined by the dot products of unit vectors. These describe pairwise distinguishabilities that can be obtained from THOM visibilities [see Fig. 1(c)]. The triple overlap of Eq. (2) reduces to $\langle a|b\rangle\langle b|c\rangle\langle c|a\rangle$ and its argument, the triad phase φ_{abc} , is given by half the solid angle subtended by the three vectors and encodes three-particle distinguishability [15].

If the qubit states are not pure then V_{abc} replaces φ_{abc} as the appropriate collective distinguishing parameter and it can be used to identify mixedness in a way that is impossible using two-photon interference. THOM dips between partially distinguishable pairs of pure photons would yield $|V_{abc}|$ that satisfies Eq. (F1) with all $r_i = 1$. If this does not hold then

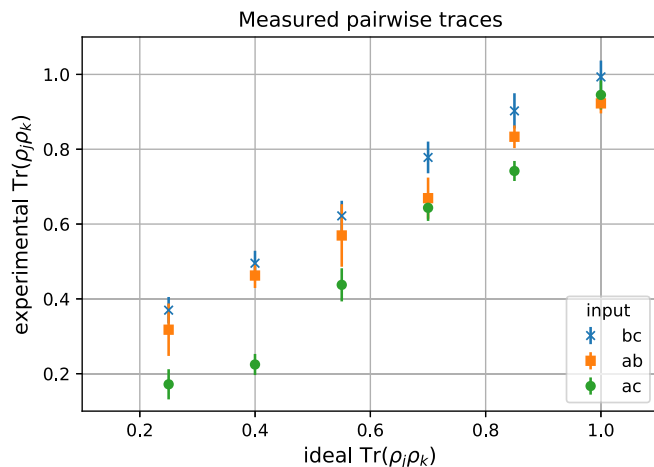


FIG. 8. Plots of the experimentally determined pairwise traces for the pure state preparation of three photons, against the ideal value from the expression $\text{Tr}(\rho_j \rho_k) = (5 + 3 \cos 2\theta)/8$ for the states in Eq. (3). Error bars indicate the standard deviation on the estimate of the pairwise trace from the three output THOM dip visibilities.

the assumption of pure states is incorrect and mixedness can be identified. It is worth noting here why qubit states are insufficient to freely tune the five distinguishing parameters for three-photon interference: knowledge of the vector dot products fixes the magnitude $|V_{abc}|$ and so the real and imaginary parts of $\text{Tr}(\rho_a \rho_b \rho_c)$ are not independent.

We now briefly describe an experiment we performed where the measured V_{abc} indicates the mixedness of an unresolved state. We prepare three photons in pure polarization states labeled $|a\rangle, |b\rangle, |c\rangle$ (with associated Bloch vectors $\mathbf{r}_j, j = a, b, c$) that ideally set the following quantities:

$$\begin{aligned} \mathbf{r}_a \cdot \mathbf{r}_b &= 0.5, \\ \mathbf{r}_a \cdot \mathbf{r}_c &= 0.27, \\ \mathbf{r}_b \cdot \mathbf{r}_c &= -0.03, \\ V_{abc} = \mathbf{r}_a \cdot (\mathbf{r}_b \times \mathbf{r}_c) &= -0.82. \end{aligned} \quad (\text{F2})$$

We then perform two sets of measurements: first, THOM dip visibilities between pairs of photons to infer experimental Bloch vector dot products [from pairwise traces, see Eq. (1)]; second, three-photon counts at the tritter outputs as the temporal delay of photon b is swept: this varies between temporal distinguishability and indistinguishability of b with respect to the other photons. The relative values of the partially bunched probabilities at these two extremes allows direct measurement of V_{abc} [using Eq. (5)].

In order to simulate the mixedness of the state ρ_a , we repeat the above measurements but now with the first photon in the pure state $|a^\perp\rangle$ which is on the opposite side of the Bloch sphere to $|a\rangle$. This flips the sign of V_{abc} above and also changes some of the dot products. We then take weighted sums of statistics for the first and second preparations of the photons to simulate state impurity for photon a .

As an example, we set the purity of the first photon to 0.9 so that the associated Bloch vector length is ideally $r_a = 0.64$. Substituting the measured values of vector dot products and $|V_{abc}|$ into Eq. (F1), we experimentally find a best estimate $r_a = 0.56$. This confirms that measurement of V_{abc} can permit identification of mixedness of a qubit state. Deviation from the ideal value mostly arises from imperfect state preparation, fitting errors due to Poissonian counting statistics and low visibility signals, and residual spectral distinguishability.

APPENDIX G: TRACE OF FOUR QUBIT STATES

The interference of four photons will depend on pairwise traces, triple traces, and also the quadruple trace $\text{Tr}(\rho_a \rho_b \rho_c \rho_d)$. For qubit states, this last quantity can be expressed in terms of Bloch vector dot and scalar triple products

$$\begin{aligned} \text{Tr}(\rho_a \rho_b \rho_c \rho_d) &= \frac{1}{8} [1 + [\mathbf{r}_a \cdot \mathbf{r}_b + \mathbf{r}_a \cdot \mathbf{r}_c + \mathbf{r}_a \cdot \mathbf{r}_d + \mathbf{r}_b \cdot \mathbf{r}_c \\ &\quad + \mathbf{r}_b \cdot \mathbf{r}_d + \mathbf{r}_c \cdot \mathbf{r}_d] + [(\mathbf{r}_a \cdot \mathbf{r}_b)(\mathbf{r}_c \cdot \mathbf{r}_d) \\ &\quad - (\mathbf{r}_a \cdot \mathbf{r}_c)(\mathbf{r}_b \cdot \mathbf{r}_d) + (\mathbf{r}_a \cdot \mathbf{r}_d)(\mathbf{r}_b \cdot \mathbf{r}_c)] \\ &\quad + i[\mathbf{r}_a \cdot (\mathbf{r}_b \times \mathbf{r}_c) + \mathbf{r}_a \cdot (\mathbf{r}_b \times \mathbf{r}_d) \\ &\quad + \mathbf{r}_a \cdot (\mathbf{r}_c \times \mathbf{r}_d) + \mathbf{r}_b \cdot (\mathbf{r}_c \times \mathbf{r}_d)]. \end{aligned} \quad (\text{G1})$$

Hence two- and three-photon parameters fully determine the interference of four photons with mixed qubit states. For qubits, higher-order traces can be decomposed into combina-

tions of dot and scalar triple products using the commutation relations for Pauli matrices: $\sigma_j \sigma_k = \delta_{jk} \mathbb{I} + i \varepsilon_{jkl} \sigma_l$.

APPENDIX H: INTERFERENCE OF THREE PHOTONS WITH QUTRIT STATES

In the main text, we concentrated on three photons with qubit states to present an intuitive geometric picture of mixedness and distinguishability. However, this imposes a restriction on the five parameters governing three-photon interference through Eqs. (2) and (F1), and as discussed in Appendix F. A three-dimensional (qutrit) space is needed to fully probe three-photon distinguishability.

The Gell-Mann matrices $\{\lambda_i\}$ are generators of the SU(3) group and satisfy commutation and anticommutation relations

$$[\lambda_r, \lambda_s] = 2i f_{rst} \lambda_t, \quad \{\lambda_s, \lambda_r\} = \frac{4}{3} \delta_{rs} + 2d_{rst} \lambda_t. \quad (\text{H1})$$

d_{rst} and f_{rst} are, respectively, the completely symmetric and antisymmetric SU(3) structure constants. These define symmetric and antisymmetric vector products [30]

$$\mathbf{a} \star \mathbf{b} := \sqrt{3} d_{rst} a_s b_t, \quad \mathbf{a} \star \mathbf{b} = \mathbf{b} \star \mathbf{a}, \quad (\text{H2})$$

$$\mathbf{a} \wedge \mathbf{b} := f_{rst} a_s b_t, \quad \mathbf{a} \wedge \mathbf{b} = -\mathbf{b} \wedge \mathbf{a}. \quad (\text{H3})$$

\mathbf{a} and \mathbf{b} are eight-dimensional real vectors that are the qutrit equivalents of Bloch vectors.

A general qutrit state ρ_j can be expressed by [30]

$$\rho_j = \frac{1}{3} (\mathbb{I} + \sqrt{3} \mathbf{n}_j \cdot \boldsymbol{\lambda}), \quad (\text{H4})$$

where $\boldsymbol{\lambda}$ is the vector of the eight Gell-Mann matrices and the components of the eight-dimensional vector $\mathbf{n}_j = \sqrt{3}/2 \times \text{Tr}(\rho_j \boldsymbol{\lambda})$. Pairwise traces of two qutrit states are, as for qubits, captured by the dot products of the associated vectors. However, the triple trace becomes considerably more complicated [30–32]:

$$\begin{aligned} \text{Tr}(\rho_a \rho_b \rho_c) &= \frac{1}{9} \left[(1 + 2(\mathbf{n}_a \cdot \mathbf{n}_b + \mathbf{n}_a \cdot \mathbf{n}_c + \mathbf{n}_b \cdot \mathbf{n}_c \right. \\ &\quad \left. + \mathbf{n}_a \cdot (\mathbf{n}_b \star \mathbf{n}_c)) + i \frac{2}{3\sqrt{3}} \mathbf{n}_a \cdot (\mathbf{n}_b \wedge \mathbf{n}_c) \right]. \end{aligned} \quad (\text{H5})$$

For qubits, we saw from Eq. (2) that the real part of the triple trace is fully determined by Bloch vector dot products. For qutrits, this no longer holds due to the presence of $\mathbf{n}_a \cdot (\mathbf{n}_b \star \mathbf{n}_c)$. It is also possible to prepare three pure qutrit states such that the pairwise traces are constant but the terms involving three \mathbf{n}_j vectors vary. see, for example, Ref. [15] or the following configuration from Ref. [31]:

$$\begin{aligned} |a\rangle &= |\mathbf{0}\rangle, \\ |b\rangle &= \frac{1}{\sqrt{2}} (|\mathbf{0}\rangle + |\mathbf{1}\rangle), \\ |c\rangle &= \frac{1}{\sqrt{3}} (|\mathbf{0}\rangle + (2e^{i\gamma} - 1)|\mathbf{1}\rangle + \sqrt{4 \cos \gamma - 3} |\mathbf{2}\rangle). \end{aligned} \quad (\text{H6})$$

The sum of the dot products is $3/4$, independent of the angle γ , but the triple trace is $e^{i\gamma}/3$.

- [1] J. L. O'Brien, A. Furusawa, and J. Vučković, Photonic quantum technologies, *Nat. Photonics* **3**, 687 (2009).
- [2] P. Kok, W. J. Munro, K. Nemoto, T. C. Ralph, J. P. Dowling, and G. J. Milburn, Linear optical quantum computing with photonic qubits, *Rev. Mod. Phys.* **79**, 135 (2007).
- [3] H.-S. Zhong, H. Wang, Y.-H. Deng, M.-C. Chen, L.-C. Peng, Y.-H. Luo, J. Qin, D. Wu, X. Ding, Y. Hu *et al.*, Quantum computational advantage using photons, *Science* **370**, 1460 (2020).
- [4] E. Polino, M. Valeri, N. Spagnolo, and F. Sciarrino, Photonic quantum metrology, *AVS Quantum Sci.* **2**, 024703 (2020).
- [5] N. Sangouard, C. Simon, H. de Riedmatten, and N. Gisin, Quantum repeaters based on atomic ensembles and linear optics, *Rev. Mod. Phys.* **83**, 33 (2011).
- [6] H. J. Kimble, The quantum internet, *Nature (London)* **453**, 1023 (2008).
- [7] M. Pompili, S. L. N. Hermans, S. Baier, H. K. C. Beukers, P. C. Humphreys, R. N. Schouten, R. F. L. Vermeulen, M. J. Tiggelman, L. dos Santos Martins, B. Dirkse, S. Wehner, and R. Hanson, Realization of a multinode quantum network of remote solid-state qubits, *Science* **372**, 259 (2021).
- [8] B.-G. Englert, Fringe visibility and which-way information: An inequality, *Phys. Rev. Lett.* **77**, 2154 (1996).
- [9] C. Dittel, G. Dufour, G. Weihs, and A. Buchleitner, Wave-particle duality of many-body quantum states, *Phys. Rev. X* **11**, 031041 (2021).
- [10] M. C. Tichy, Sampling of partially distinguishable bosons and the relation to the multidimensional permanent, *Phys. Rev. A* **91**, 022316 (2015).
- [11] M. Tillmann, S.-H. Tan, S. E. Stoeckl, B. C. Sanders, H. de Guise, R. Heilmann, S. Nolte, A. Szameit, and P. Walther, Generalized multiphoton quantum interference, *Phys. Rev. X* **5**, 041015 (2015).
- [12] V. S. Shchesnovich, Partial indistinguishability theory for multiphoton experiments in multiport devices, *Phys. Rev. A* **91**, 013844 (2015).
- [13] V. S. Shchesnovich and M. E. O. Bezerra, Collective phases of identical particles interfering on linear multiports, *Phys. Rev. A* **98**, 033805 (2018).
- [14] J. J. Renema, A. Menssen, W. R. Clements, G. Triginer, W. S. Kolthammer, and I. A. Walmsley, Efficient classical algorithm for boson sampling with partially distinguishable photons, *Phys. Rev. Lett.* **120**, 220502 (2018).
- [15] A. J. Menssen, A. E. Jones, B. J. Metcalf, M. C. Tichy, S. Barz, W. S. Kolthammer, and I. A. Walmsley, Distinguishability and many-particle interference, *Phys. Rev. Lett.* **118**, 153603 (2017).
- [16] A. E. Jones, A. J. Menssen, H. M. Chrzanowski, T. A. W. Wolterink, V. S. Shchesnovich, and I. A. Walmsley, Multiparticle interference of pairwise distinguishable photons, *Phys. Rev. Lett.* **125**, 123603 (2020).
- [17] A. M. Minke, A. Buchleitner, and C. Dittel, Characterizing four-body indistinguishability via symmetries, *New J. Phys.* **23**, 073028 (2021).
- [18] D. J. Brod, E. F. Galvão, N. Viggianiello, F. Flamini, N. Spagnolo, and F. Sciarrino, Witnessing genuine multiphoton indistinguishability, *Phys. Rev. Lett.* **122**, 063602 (2019).
- [19] N. Viggianiello, F. Flamini, M. Bentivegna, N. Spagnolo, A. Crespi, D. J. Brod, E. F. Galvão, R. Osellame, and F. Sciarrino, Optimal photonic indistinguishability tests in multimode networks, *Sci. Bull.* **63**, 1470 (2018).
- [20] M. Pont, R. Albiero, S. E. Thomas, N. Spagnolo, F. Ceccarelli, G. Corrielli, A. Brioussel, N. Somaschi, H. Huet, A. Harouri, A. Lemaître, I. Sagnes, N. Belabas, F. Sciarrino, R. Osellame, P. Senellart, and A. Crespi, Quantifying n -photon indistinguishability with a cyclic integrated interferometer, *Phys. Rev. X* **12**, 031033 (2022).
- [21] S. Agne, J. Jin, J. Z. Salvail, K. J. Resch, T. Kauten, E. Meyer-Scott, D. R. Hamel, G. Weihs, and T. Jennewein, Observation of genuine three-photon interference, *Phys. Rev. Lett.* **118**, 153602 (2017).
- [22] O. F. Thomas, W. McCutcheon, and D. P. McCutcheon, A general framework for multimode gaussian quantum optics and photo-detection: Application to hong-ou-mandel interference with filtered heralded single photon sources, *APL Photonics* **6**, 040801 (2021).
- [23] J. Shi and T. Byrnes, Effect of partial distinguishability on quantum supremacy in gaussian boson sampling, *npj Quantum Inf.* **8**, 54 (2022).
- [24] M. R. Barros, S. Chin, T. Pramanik, H.-T. Lim, Y.-W. Cho, J. Huh, and Y.-S. Kim, Entangling bosons through particle indistinguishability and spatial overlap, *Opt. Express* **28**, 38083 (2020).
- [25] C. K. Hong, Z. Y. Ou, and L. Mandel, Measurement of subpicosecond time intervals between two photons by interference, *Phys. Rev. Lett.* **59**, 2044 (1987).
- [26] F. Bouchard, A. Sit, Y. Zhang, R. Fickler, F. M. Miatto, Y. Yao, F. Sciarrino, and E. Karimi, Two-photon interference: The hong-ou-mandel effect, *Rep. Prog. Phys.* **84**, 012402 (2021).
- [27] P. P. Rohde, Boson sampling with photons of arbitrary spectral structure, *Phys. Rev. A* **91**, 012307 (2015).
- [28] S. Stanisic and P. S. Turner, Discriminating distinguishability, *Phys. Rev. A* **98**, 043839 (2018).
- [29] This can be obtained using the identity $\sigma_i \sigma_j = \delta_{ij} \mathbb{I} + i \varepsilon_{ijk} \sigma_k$.
- [30] Arvind, K. S. Malleth, and N. Mukunda, A generalized pancharatnam geometric phase formula for three-level quantum systems, *J. Phys. A: Math. Gen.* **30**, 2417 (1997).
- [31] J. Hartley and V. Vedral, Entropy as a function of geometric phase, *J. Phys. A: Math. Gen.* **37**, 11259 (2004).
- [32] C. M. Caves and G. J. Milburn, Qutrit entanglement, *Opt. Commun.* **179**, 439 (2000).
- [33] C. Sparrow, Quantum interference in universal linear optical devices for quantum computation and simulation, Ph.D. thesis, Imperial College London, 2017.
- [34] H.-S. Zhong, Y.-H. Deng, J. Qin, H. Wang, M.-C. Chen, L.-C. Peng, Y.-H. Luo, D. Wu, S.-Q. Gong, H. Su *et al.*, Phase-programmable gaussian boson sampling using stimulated squeezed light, *Phys. Rev. Lett.* **127**, 180502 (2021).
- [35] R. Raussendorf, D. E. Browne, and H. J. Briegel, Measurement-based quantum computation on cluster states, *Phys. Rev. A* **68**, 022312 (2003).
- [36] M. Gimeno-Segovia, P. Shadbolt, D. E. Browne, and T. Rudolph, From three-photon Greenberger-Horne-Zeilinger states to ballistic universal quantum computation, *Phys. Rev. Lett.* **115**, 020502 (2015).
- [37] P. P. Rohde and T. C. Ralph, Error models for mode mismatch

- in linear optics quantum computing, *Phys. Rev. A* **73**, 062312 (2006).
- [38] T. Tilma and E. C. G. Sudarshan, Generalized euler angle parametrization for $SU(N)$, *J. Phys. A: Math. Gen.* **35**, 10467 (2002).
- [39] Sinkhorn-knopp PYTHON implementation, https://github.com/btaba/sinkhorn_knopp.
- [40] J. Casey, *A Treatise on Spherical Trigonometry* (Hodges, Figgis & Co., Dublin, 1889).